

JGR Solid Earth

RESEARCH ARTICLE

10.1029/2019JB018698

Special Section:

Ophiolites and Oceanic Lithosphere, with a focus on the Samail ophiolite in Oman

Key Points:

- Brine-saturated resistivity is systematically lower than dry resistivity, with the differences attributed to the volume fraction of pores
- Permeability through the crust-mantle sequences was modeled using the effective medium theory and resistivity data
- The dunite sequence is characterized by higher permeability than the overlying gabbro and underlying harzburgite sequences

Correspondence to:

I. Katayama,
katayama@hiroshima-u.ac.jp

Citation:

Katayama, I., Abe, N., Hatakeyama, K., Akamatsu, Y., Okazaki, K., & Ulven, O. I., et al. (2020). Permeability profiles across the crust-mantle sections in the Oman Drilling Project inferred from dry and wet resistivity data. *Journal of Geophysical Research: Solid Earth*, 125, e2019JB018698. <https://doi.org/10.1029/2019JB018698>

Received 18 SEP 2019

Accepted 7 APR 2020

Accepted article online 27 JUN 2020

Permeability Profiles Across the Crust-Mantle Sections in the Oman Drilling Project Inferred From Dry and Wet Resistivity Data

Ikuo Katayama¹ , Natsue Abe² , Kohei Hatakeyama¹ , Yuya Akamatsu¹, Keishi Okazaki³, Ole Ivar Ulven⁴ , Gilbert Hong⁵ , Wenlu Zhu⁶ , Benoit Cordonnier⁴, Katsuyoshi Michibayashi⁷, Marguerite Godard⁸ , and Peter Kelemen⁹

¹Department of Earth and Planetary Systems Science, Hiroshima University, Hiroshima, Japan, ²Mantle Drilling Promotion Office, MarE3, JAMSTEC, Kanagawa, Japan, ³Kochi Institute for Core Sample Research, JAMSTEC, Kochi, Japan, ⁴Department of Geosciences, University of Oslo, Oslo, Norway, ⁵Earth and Environmental Sciences, Seoul National University, Seoul, South Korea, ⁶Department of Geology, University of Maryland, College Park, MD, USA, ⁷Department of Earth and Planetary Sciences, Nagoya University, Aichi, Japan, ⁸Géosciences Montpellier, CNRS, Université de Montpellier, Montpellier, France, ⁹Lamont Doherty Earth Observatory, Columbia University, New York, NY, USA

Abstract Permeability profiles in the crust-mantle sequences of the Samail ophiolite were constructed based on onboard measurements of the electrical resistivity of cores recovered during the Oman Drilling Project. For each sample, we measured dry and brine-saturated resistivity during the description campaign on the drilling vessel *Chikyu*. Owing to the conductive brine in the pore space, wet resistivity is systematically lower than dry resistivity. The difference between dry and wet resistivity is attributed to the movement of dissolved ions in brine that occupies the pore space. We applied effective medium theory to calculate the volume fraction of pores that contribute to electrical transport. Using an empirical cubic law between transport porosity and permeability, we constructed permeability profiles for the crust-mantle transition zone and the serpentinized mantle sections in the Samail ophiolite. The results indicate that (1) the gabbro sequence has a markedly lower permeability than the underlying mantle sequence; (2) serpentinized dunites have higher permeability than serpentinized harzburgites; and (3) discrete sample permeability is correlated with ultrasonic velocity, suggesting that the permeability variations predominately reflect crack density and geometry.

Plain Language Summary Aqueous fluids that circulated beneath the seafloor play an important role in heat transfer, chemical exchange, and microbial activity in the oceanic lithosphere. The Oman Drilling Project was successful in obtaining continuous drill cores through the crust-mantle sequences in the Samail ophiolite, where the paleo-oceanic basement was thrust onto the continental crust in the Late Cretaceous. In this study, we constructed profiles of permeability across the crust-mantle sections using the effective medium theory and resistivity data, which provide insights into fluid circulation in the oceanic lithosphere. The results indicate higher permeability in the uppermost mantle sequence between the crust and the underlying mantle, suggesting that present-day fluid transfer is predominant at the crust-mantle boundary. Although the fluid flow and chemical reactions are likely coupled, the high permeability could promote the transformation of crust-mantle materials and hence the recycling of water into the mantle. Application of this technique to forthcoming deep drilling projects through the Mohorovičić discontinuity (Moho) and into the upper mantle may provide insights into the permeability structure and fluid circulation system in the oceanic lithosphere.

1. Introduction

Permeability is a key control on heat and chemical exchange in the oceanic lithosphere, as well as microbial activity in the subseafloor (e.g., Fisher, 1998; Furnes et al., 2001; Stein & Stein, 1994). In investigations based on ocean drilling projects, the permeability is often inferred from resistivity data because electrical transport at the crustal depths is controlled mainly by fluid flow. This approach uses an empirical relationship between resistivity and porosity, such as Archie's law (e.g., Gueguen & Palciauskas, 1994), and models the permeability from resistivity logging data and/or resistivity measurements of recovered core samples (e.g.,

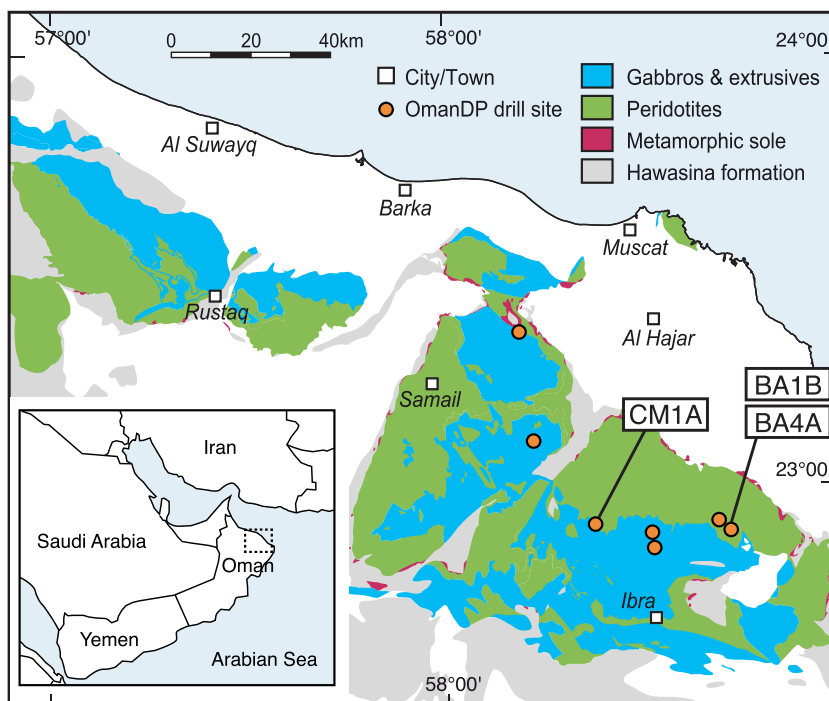


Figure 1. Geological map of the southeastern massif of the Samail ophiolite (after Nicolas et al., 2000) showing the drill site locations of the Oman Drilling Projects. The colored units are the ophiolite sequence. The inset shows a map of the Arabian Peninsula, in which the location of the main figure is indicated by the dashed box.

Anderson et al., 1985; Becker et al., 1982; Carlson, 2011; Slagle & Goldberg, 2011). Archie's law is valid for a conducting phase that saturates a nonconducting matrix. However, when the matrix has a significant conductivity, the Archie's law is no longer applicable (Glover et al., 2000). In serpentinitized ultramafic sequences, hydration reactions are commonly associated with the production of magnetite, which is a highly conductive material. As a result, the conductivity of the serpentinitized matrix varies with the degree of hydration and chemical exchanges (e.g., Stesky & Brace, 1973).

We carried out systematic measurements of dry and wet resistivity on core samples collected during the Oman Drilling Project from the crust to mantle of the Samail ophiolite. Using effective medium theory (e.g., Mavko et al., 2009), we calculated the permeability based on the brine-saturated and matrix resistivities, and determined the relative changes of permeability across crust-mantle sections in the Samail ophiolite. We show that this approach can be used to construct a first-order permeability profile during oceanic drilling programs, although the permeability can be heterogeneous in the oceanic lithosphere and scaling effects need to be evaluated.

2. Core Samples and Methods

The Oman Drilling Project obtained nine diamond-cored boreholes through the Samail ophiolite from the dike-gabbro transition to the uppermost mantle (Figure 1). The total cumulative drilled core length is 5,458 m with ~100% core recovery (Kelemen et al., 2018; Teagle et al., 2018). In this study, we focused on three boreholes (CM1A, BA1B, and BA4A) that are each ~300–400 m long. Hole CM1A samples the crust-mantle transition from layered gabbros through dunites into harzburgites of the upper mantle sequences. Hole BA1B comprises dunite (upper section) and harzburgite (lower section) cut by numerous mafic dikes. Hole BA4A consists dominantly of dunite with minor harzburgite and is crosscut by abundant mafic dikes. The mantle sequences are highly altered, with >70% serpentinitization, and contain few relicts of primary olivine and orthopyroxene. The recovered core samples were systematically analyzed on the drilling vessel *Chikyu* during the description campaigns in 2017 and 2018, including mineralogical, geochemical, structural, and geophysical analyses (Kelemen et al., 2018). Electrical resistivity, ultrasonic velocity,

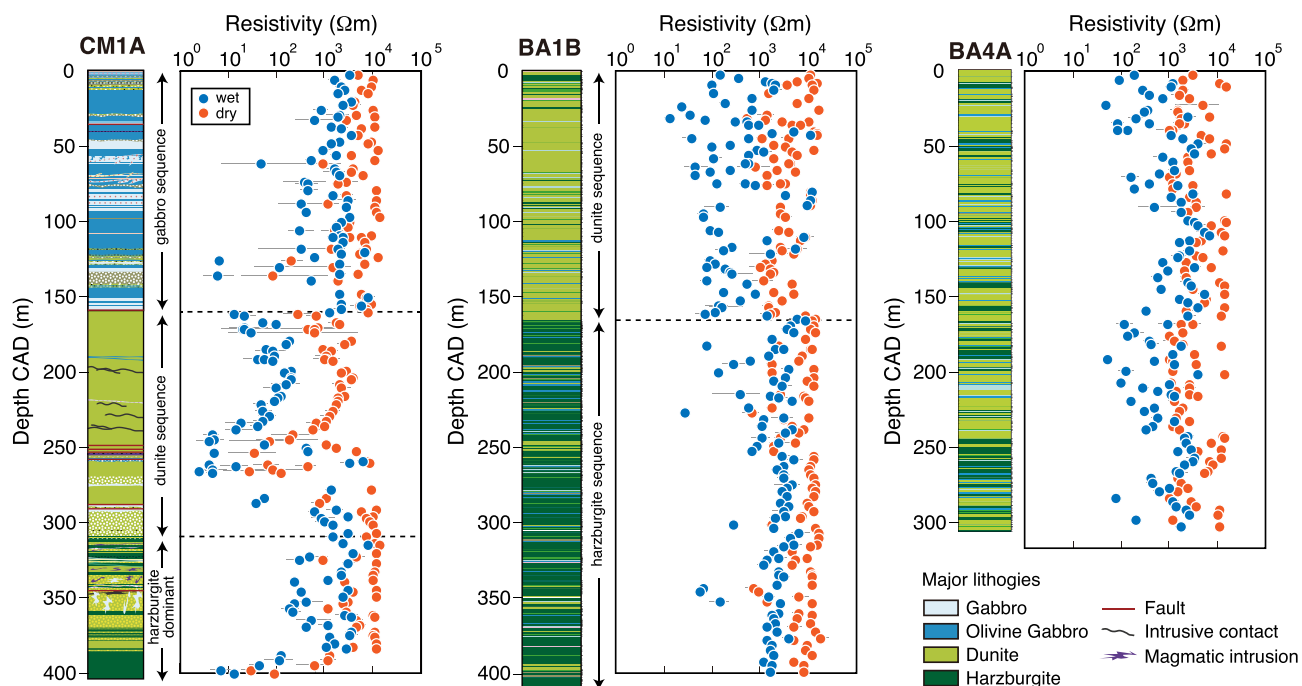


Figure 2. Down-hole plots of resistivity in the three boreholes (CM1A, BA1B, and BA4A), and borehole stratigraphy. Blue and red circles indicate measurements under wet and dry conditions, respectively. The data represent the averaged resistivities in three orthogonal orientations, and the bars indicate the variations in the measurement directions.

bulk/grain density, porosity, and thermal conductivity were measured on selected discrete samples (Abe et al., 2018).

The core samples were cut into $\sim 2 \times 2 \times 2$ cm cubes, in which the x and y directions were perpendicular and parallel to the split surface of the working halves, respectively, and the z direction was the down-hole axis. For the wet measurements, samples were saturated with NaCl solution (3.5 g/L), equivalent to the salinity in bore-hole water measured in the field (Paukert et al., 2012). The resistivity was measured in three orthogonal directions using an Agilent 4294A Procession Impedance Analyzer with a set of two stainless steel electrodes. Measurements were carried at laboratory temperatures of 22.5 to 23.3°C, resulting in a temperature-induced resistivity variation of $\sim 1\%$, which is broadly equivalent to the accuracy of sample dimensions. Two paper filters soaked in brine for wet measurements and two stainless steel mesh filters for dry measurements were placed between the steel electrodes and sample cube on its topside and bottomside to enhance coupling. The magnitude ($|Z|$) and phase angle (θ) of the complex impedance were measured at 25 kHz across the array from 40 Hz to 10 MHz. The resistivity was calculated from the sample impedance, length, and cross-sectional area in each orientation. Blank tests yielded ~ 20 k Ω m, which is the upper limit of the resistivity measurements. The detailed methodology of the resistivity measurements was described by Hatakeyama et al. (2015).

3. Resistivity Data

The electrical resistivity results from Holes CM1A, BA1B, and BA4A are shown as a down-hole plot in Figure 2. Circles indicate the averaged resistivity, and bars represent the variation in the three orthogonal directions. Although some samples exhibit large variations with measurement orientations, the resistivity anisotropy is relatively weak in each borehole and there are no systematic variations with orientation (Figure 3). Dry resistivity varies from 26Ω m to 13 k Ω m in Hole CM1A, 525Ω m to 18 k Ω m in Hole BA1B, and 952Ω m to 15 k Ω m in Hole BA4A (the geometric mean and standard deviation of each sequence are listed in Table 1). Although the resistivities in the dry measurements nearly reached the upper limit of the measurement system, the large variations can be attributed to mineralogical and textural variations, such as the occurrence and connectivity of conductive phases. Wet resistivity varies from 2.5Ω m to

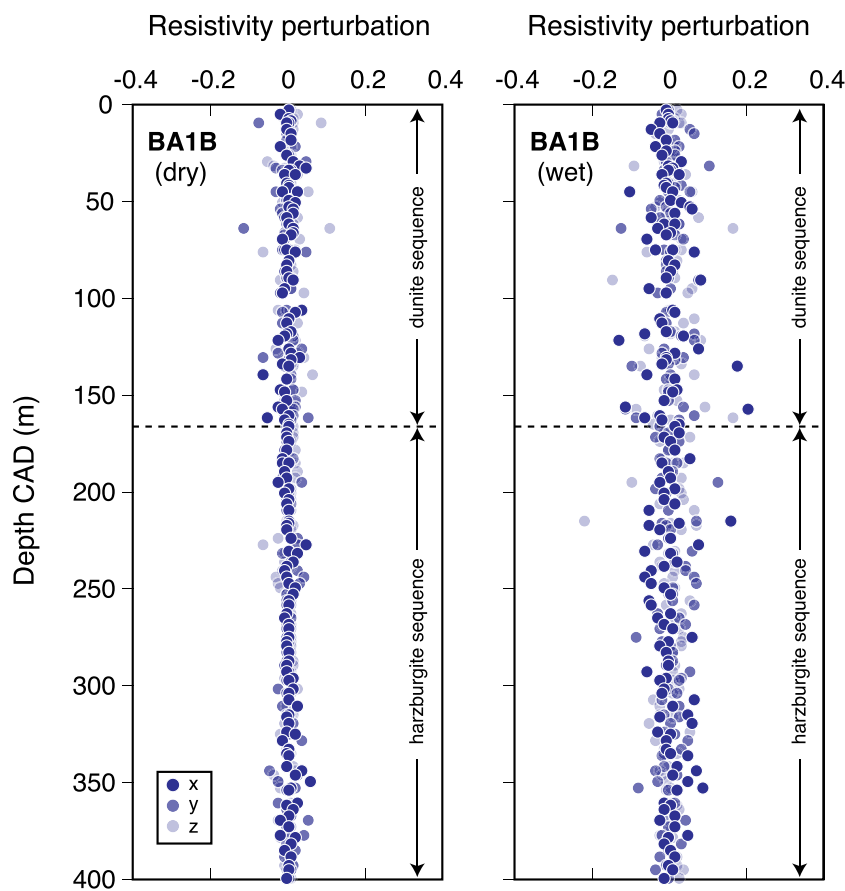


Figure 3. Resistivity perturbations of dry and wet measurements in Hole BA1B. Perturbations were calculated as $(\log R_i - \log \bar{R}) / \log \bar{R}$, where R_i is the resistivity of each orientation and \bar{R} is the averaged resistivity of the three orthogonal orientations.

7.7 k Ω m in Hole CM1A, 13 Ω m to 12 k Ω m in Hole BA1B, and 48 Ω m to 6.4 k Ω m in Hole BA4A, and is systematically lower than the dry resistivity in each borehole (Table 1).

The gabbro sequence has a nearly constant and high resistivity, with occasional low resistivity related to layers of wehrlite and dunite. In the mantle section, the dunite-dominant sequence has a relatively low resistivity, consistent with the high degree of alternation in dunite as compared to harzburgite. Mafic dikes in the upper mantle section have a high resistivity, similar to similar lithologies in the gabbro sequence. The brine-saturated resistivity generally shows trends similar to the dry measurements, but is systematically lower than dry

Table 1
Mean Resistivity and Calculated Transport Porosity and Permeability in Each Borehole

| | | Resistivity (Ω m) | | Transport porosity (%) | Permeability (m^2) |
|------|----------------------|---------------------------|--------------------------|------------------------|------------------------------|
| | | Dry | Wet | | |
| CM1A | Gabbro sequence | 4.94×10^3 (2.4) | 1.23×10^3 (4.0) | 0.12 (2.9) | 5.39×10^{-21} (200) |
| | Dunite sequence | 1.10×10^3 (4.4) | 6.60×10^1 (6.6) | 3.43 (6.9) | 2.00×10^{-17} (331) |
| | Harzburgite sequence | 3.45×10^3 (4.6) | 5.44×10^2 (5.9) | 0.38 (6.2) | 2.44×10^{-20} (245) |
| BA1B | Dunite sequence | 3.27×10^3 (2.4) | 3.13×10^2 (4.9) | 0.63 (7.1) | 2.26×10^{-19} (354) |
| | Harzburgite sequence | 6.86×10^3 (2.2) | 1.56×10^3 (3.0) | 0.12 (3.3) | 1.57×10^{-21} (36) |
| BA4A | Dunite sequence | 2.38×10^3 (2.1) | 5.20×10^2 (3.2) | 0.34 (3.9) | 3.77×10^{-20} (61) |

Note. Mean values were calculated the geometric mean, and the number in parentheses represents the geometric standard deviation.

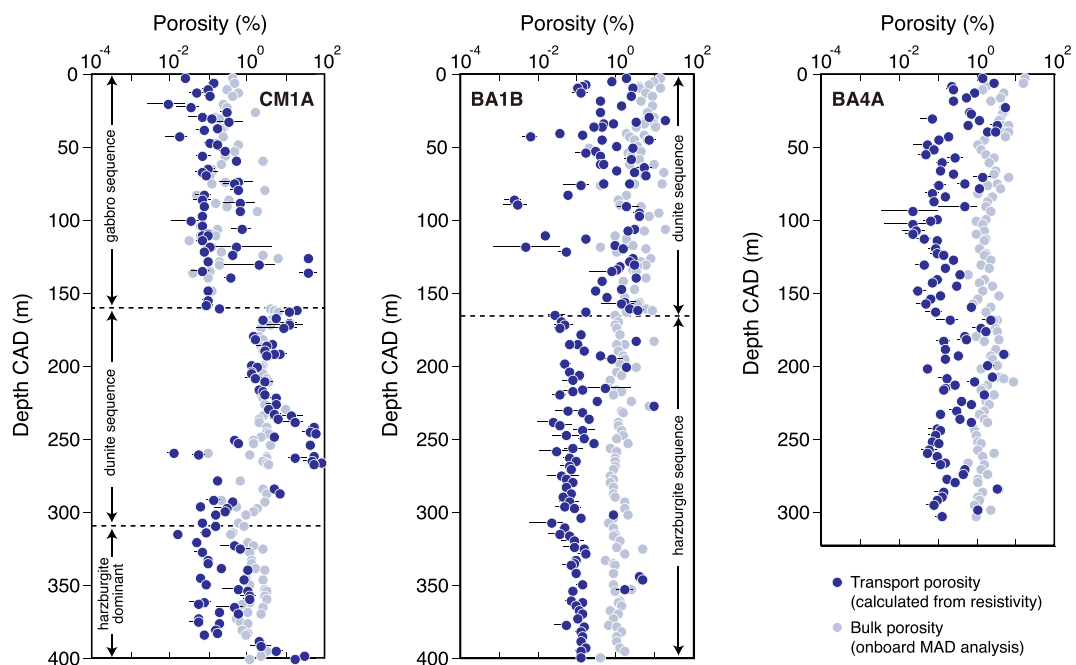


Figure 4. Profiles of transport porosity calculated from the wet and dry resistivities. The data represent the averaged porosities in three orthogonal orientations, and bars indicate the range of values in all measurement directions. Gray symbols indicate the bulk porosity estimated from the moisture and density (MAD) analyses during the description campaign (Abe et al., 2018), and are mostly higher than the calculated porosity.

resistivity due to the presence of conductive brine in the pore space (Figure 2). The difference between wet and dry resistivity is related to the pore volume and geometry, as discussed in the following section.

4. Permeability Profile

Given that the dry matrix has significant variations in resistivity, due in part to the presence of variable amounts of magnetite associated with serpentinization, Archie's law is not applicable to these data. Therefore, we used the Hashin-Shtrikman upper bound (e.g., Mavko et al., 2009) to estimate the volume fraction of pores that contribute to electrical transport (termed "transport porosity") as follows:

$$\sigma_{eff} = \sigma_f \left(1 - \frac{3(1-\phi)(\sigma_f - \sigma_{dry})}{3\sigma_f - \phi(\sigma_f - \sigma_{dry})} \right),$$

where σ_{eff} , σ_f , and σ_{dry} are the effective, fluid, and dry conductivity (inverse of resistivity), respectively, and ϕ is the transport porosity. The effective conductivity corresponds to the wet measurement, and the fluid conductivity was set to 0.58 S/m based in its salinity (Carmichael, 1982). Figure 4 shows profiles of the calculated transport porosity in each borehole. The transport porosity inferred from the difference between the brine-saturated and dry resistivities is generally lower than the bulk porosity that was estimated from the moisture and density analysis. Some samples have an extremely high transport porosity because they have a low matrix resistivity (i.e., high conductivity) that is close to the fluid resistivity. Moreover, if a sample have a relatively small difference between wet and dry resistivity, then the calculated transport porosity has a relatively large uncertainty.

There are several other models that describe multiphase conducting mixtures. We also applied a modified version of Archie's law that incorporates the effect of matrix resistivity, as follows:

$$\sigma_{eff} = \sigma_{dry}(1-\phi)^{\log(1-\phi^m)/\log(1-\phi)} + \sigma_f \phi^m,$$

where m is the cementation exponent (Glover et al., 2000). The results are almost identical to the calculations using the Hashin-Shtrikman upper bound, if an exponent of $m = 1$ is used, although the large

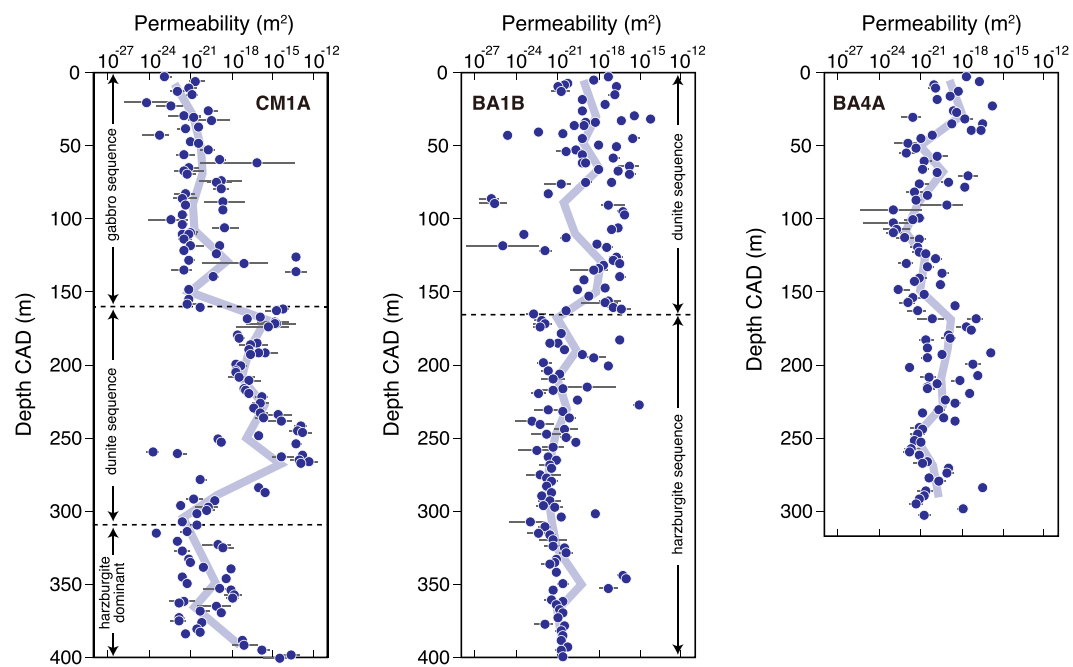


Figure 5. Profiles of permeability calculated from resistivity data using the effective medium theory. The data represent the averaged permeabilities in three orthogonal orientations, and the bars indicate the variations in the measurement directions. Gray lines are the 20 m averaged permeability profiles.

exponent in the modified Archie's law yields a higher porosity that exceeds those inferred from the moisture and density analysis.

We then approximated an empirical relationship between transport porosity (ϕ) and permeability (k), as follows:

$$k = A\phi^n,$$

where A is a constant and the exponent n is related to pore geometry (e.g., Gueguen & Palciauskas, 1994). A geometric exponent of $n = 3$ was used in our calculations, because the pores are approximately planar cracks in these samples, as revealed by ultrasonic measurements and structural observations during the onboard core description (Abe et al., 2018; Kelemen et al., 2018).

To check and calibrate our calculations, we conducted a direct measurement of permeability using an intravessel fluid flow apparatus, applying a constant pressure gradient in the core sample (for details, see Katayama et al., 2012). This yielded a permeability of $5.1 \times 10^{-19} \text{ m}^2$ for a dunite sample with 0.8% porosity inferred from the resistivity data. This permeability is similar to those of low-temperature serpentinites collected from the accretionary prism of the Mineoka belts, but slightly lower than those of dredged samples from the ocean floors (Hatakeyama et al., 2017). Based on this benchmarking test, we obtained $A = 9.2 \times 10^{-13}$, which was used to calculate permeability from the transport porosity. Though it is treated as a constant, this term may vary throughout the section, although the variation is usually less than one order of magnitude (Carlson, 2011). Given that the permeability is proportional to the cube of the porosity, the overall permeability profile is not sensitive to the constant term A , and is sensitive to the transport porosity.

Figure 5 shows a down-hole plot of permeability in boreholes CM1A, BA1B, and BA4A. Although the data are somewhat scattered, the calculated permeability clearly increases from the gabbro to serpentized dunite sequences, and then decreases from the dunite to serpentized harzburgite-dominated sequences in Hole CM1A. The decrease in permeability from the dunite to harzburgite layers is also observed in Hole BA1B, and this trend is consistent with the relatively low permeability of the harzburgite layers in Hole BA4A. In the crustal sections, wehrlite and dunite layers locally exhibit high permeability and, in the mantle sections, the gabbroic dikes have lower permeability than their surrounding ultramafic host rocks. The

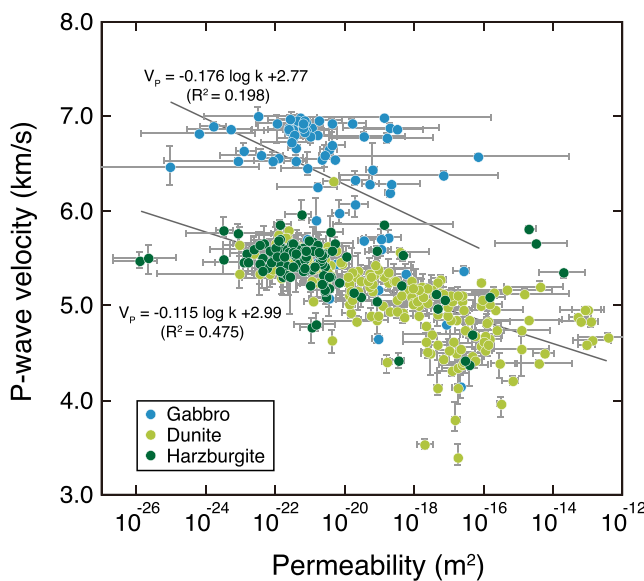


Figure 6. Relationship between calculated permeability and P wave velocity for gabbro, dunite, and harzburgite from boreholes CM1A, BA1B, and BA4A. The gabbro samples include olivine gabbro and rodingitized samples. The ultrasonic velocity was measured with an acoustic transducer of 230 kHz. Bars on the discrete data indicate the variations in the measurement orientations. Fitting curves are shown for gabbroic and ultramafic rocks.

permeability structure is also affected by fault zones, in which high permeability is associated with the presence of abundant fractures. However, highly damaged samples from fault zones were difficult to prepare for analysis, and we may overlook the presence of fracture zones in these profiles.

It is important to note that permeability can be affected by many variables; consequently, the modeled absolute values of permeability have large uncertainties. However, the relative permeability changes are robust, because transport porosity is a primary variable that reflects the electrical transport and fluid flow.

5. Relationship Between Permeability and Velocity

The calculated permeability variations are caused primarily by the different pore volumes and geometries in the analyzed core samples. Figure 6 shows the relationship between the calculated permeability and P wave velocity measured onboard during the core description campaigns. The elastic wave velocity of the ultramafic rocks is significantly lower than that of the gabbro and unaltered peridotite due to extensive serpentinization. A negative correlation between permeability and velocity is observed for the ultramafic rocks, whereby dunites are characterized by large permeability and velocity variations as compared to harzburgites (Figure 6). The gabbros exhibit a similar, although weak, correlation that might reflect the limited velocity variations. In the Holes 504B and 1256D, a similar negative correlation between model permeability and ultrasonic velocity has been reported based on logging data (Carlson, 2014).

Since the P wave velocity of low-temperature serpentinite is ~ 5 km/s (e.g., Christensen, 2004), the variations in ultrasonic velocity are potentially related to crack density, as well as the degree of alteration. Violay et al. (2010) reported that resistivity and velocity are also associated with microcracks in gabbro sampled in the Hole 1256D. The development of a crack network significantly modifies the hydrological properties, with theoretical models predicting that permeability is related to the fraction of crack, crack density, and crack radius (e.g., Simpson et al., 2001). This implies that permeability variations obtained in this study are controlled primarily by damage in the samples, possibly related to volume expansion during hydration reactions such as serpentinization. Following from MacDonald and Fyfe (1985) and O'Hanley (1992), several recent papers have suggested that, once aqueous fluids access to rocks, the volume change due to hydration can result in fracture development, maintaining or increasing permeability and reactive surface in a positive feedback (e.g., Jamtveit et al., 2008; Kelemen & Hirth, 2012; Malvoisin et al., 2017; Rudge et al., 2010; Shimizu & Okamoto, 2016; Ulven et al., 2014; Uno et al., 2019; Zheng et al., 2018; Zhu et al., 2016).

6. Comparison With a Hydrological Model and Other Oceanic Drilling Sites

In the Samail ophiolite, hydrological analyses have been undertaken using stream-flow gauging and the chemical dilution method (Dewandel et al., 2005). These approaches indicated that fluid flow is more efficient in gabbro and dolerite than in peridotite. Although the hydrological results are different from the intrinsic permeability inferred from our resistivity measurements, groundwater circulation in the hydrological models is dominated by flow in a fissured near-surface horizon (<50 m depth). At such depths, frequently observed joints and fractures are probably the main conduits for fluid flow, while such features do not affect our resistivity measurements on discrete core samples.

In the shallow oceanic crusts, in situ permeability is often measured using borehole packer tests, which indicate a decrease in permeability with depth down to $\sim 10^{-17}$ m 2 in the upper crust (e.g., Fisher, 1998). This is generally consistent with electrical resistivity logging data, whereby the apparent resistivity increases significantly from pillow lavas to sheeted dikes and to massive units (e.g., Becker, 1989). The sharp increase in resistivity in the underlying dike unit has been interpreted as reflecting a significant reduction in porosity that limited hydrothermal circulation in the oceanic crust (Becker et al., 1982). Carlson (2011) applied

Archie's law to the resistivity logging data obtained from Holes 504B and 1256D, and suggested that the permeability decreases from the pillow lavas ($\sim 10^{-14} \text{ m}^{-2}$) to the sheeted dikes ($\sim 10^{-18} \text{ m}^{-2}$).

Although Archie's law can be applied to the mafic section of oceanic crust, due to its nearly nonconductive matrix, it is not suitable for application to the mantle sequence because of the sensitivity of matrix resistivity to the formation of magnetite associated with serpentinization. We used effective medium theory to model the permeability in crust-mantle sections in the Samail ophiolite. Our analysis yields permeabilities for the gabbro cores of 10^{-19} to 10^{-21} m^{-2} , which are slightly lower than those of the sheeted dike unit in Holes 504B and 1256D. However, this range of permeability is consistent with direct permeability measurements on gabbro core collected from Hole 1256D (Gilbert & Bona, 2016). Our calculated permeabilities show a marked increase in the dunite sequence. These samples are extensively altered, and the permeability in the dunite and harzburgite sequences sampled by the Oman Drilling Project was likely modified during serpentinization.

Although our core-scale measurements do not show a systematic correlation in resistivity in the discrete orientations, recent active-source electromagnetic measurements have shown a clear electrical anisotropy in the oceanic lithosphere, whereby conduction at crustal depths is enhanced in a direction subparallel to the paleo mid-oceanic ridge (Chesley et al., 2019). Fisher (1998) noted that the permeability of oceanic crust varies extensively due to the presence of fractures, and cannot simply be determined from core measurements. We agree with this caveat regarding the scale-dependence of permeability, and thus the electrical resistivity in the oceanic lithosphere. Nevertheless, our analysis shows that core-scale permeability varies with lithology and structure. These data provide the first clue of the background intrinsic permeability through altered oceanic crust into serpentinized mantle sequences.

7. Conclusions

We modeled the permeability across the crust-mantle sections sampled by the Oman Drilling Project using dry and wet resistivity data and effective medium theory. Although the absolute values of the calculated permeabilities are highly uncertain, the relative permeability variations are robust. The dunite sequence has markedly higher permeability than the overlying gabbro and underlying harzburgite sequences, which is likely correlated with crack density and geometries, as well as the degree of alteration. The proposed Mohole-to-Mantle (M2M) project aims to drill through the Moho and into the upper mantle using the riser drilling vessel *Chikyu* (e.g., Umino et al., 2012). Application of our technique to core samples, as well as down-hole geophysical logging data, in this forthcoming project will provide insights into the permeability structure and fluid circulation system in the oceanic lithosphere.

Acknowledgments

We thank the science party of the Oman Drilling Project, and all those who conducted the drilling and supported the description campaign at *Chikyu*. We also thank Al-Amri Salim for assistance with the resistivity measurements. Comments from two anonymous reviewers greatly improved the manuscript. This study was supported by the Japan Society for the Promotion of Science (16H06347, 18H01321, and 18H03733). The data availability at <https://doi.org/10.1594/PANGAEA.913501>.

References

- Abe, N., Okazaki, K., Katayama, I., Hatakeyama, K., Ulven, O. I., Hong, G., et al. (2018). Initial report of physical property measurements, ChikyuOman 2018: Crust-mantle boundary and the mantle section from ICDP Oman Drilling Project Phase II. In *Paper presented at American Geophysical Union Fall Meeting, V13E-0150*. Washington D.C. USA.
- Anderson, R., Zoback, M., Hickman, S., & Newmark, R. (1985). Permeability versus depth in the upper oceanic crust: In-situ measurements in DSDP Hole 504B, eastern equatorial Pacific. *Journal of Geophysical Research*, 90(B5), 3659–3669. <https://doi.org/10.1029/JB090iB05p03659>
- Becker, K. (1989). Measurements of the permeability of the sheeted dikes in Hole 504B, ODP Leg 111. *Proceeding of the Ocean Drilling Program, Scientific Results*, 111, 317–325. <https://doi.org/10.2973/odp.proc.sr.111.156.1989>
- Becker, K., Von Herzen, R., Francis, T., Anderson, R., Honnorez, J., Adamson, A., et al. (1982). In situ electrical resistivity and bulk porosity of the oceanic crust Costa Rica Rift. *Nature*, 300, 594–598. <https://doi.org/10.1038/300594a0>
- Carlson, R. L. (2011). The effect of hydrothermal alteration on the seismic structure of the upper oceanic crust: Evidence from Holes 504B and 1256D. *Geochemistry, Geophysics, Geosystems*, 12, Q09013. <https://doi.org/10.1029/2011GC003624>
- Carlson, R. L. (2014). The influence of porosity and crack morphology on seismic velocity and permeability in the upper oceanic crust. *Geochemistry, Geophysics, Geosystems*, 15, 10–27. <https://doi.org/10.1002/2013GC004965>
- Carmichael, R. S. (1982). *Handbook of Physical Property of Rocks* (Vol. 1). Boca Raton: CRC Press.
- Chesley, C., Key, K., Constable, S., Behrens, J. P., & MacGregor, L. M. (2019). Crustal cracks and frozen flow in oceanic lithosphere inferred from electrical anisotropy. *Geochemistry, Geophysics, Geosystems*, 20, 5979–5999. <https://doi.org/10.1029/2019GC008628>
- Christensen, N. I. (2004). Serpentinites, peridotites, and seismology. *International Geology Review*, 46(9), 795–816. <https://doi.org/10.2747/0020-6814.46.9.795>
- Dewandel, B., Lachassagne, P., Boudier, F., Al-Hattali, S., Ladouce, B., Pinault, J. L., & Al-Suleimani, Z. (2005). A conceptual hydrogeological model of ophiolite hard-rock aquifers in Oman based on a multiscale and a multidisciplinary approach. *Hydrogeology Journal*, 13(5–6), 708–726. <https://doi.org/10.1007/s10040-005-0449-2>
- Fisher, A. T. (1998). Permeability within basaltic oceanic crust. *Reviews of Geophysics*, 36, 143–182. <https://doi.org/10.1029/97RG02916>

- Furnes, H., Muehlenbachs, K., Torsvik, T., Thorseth, I. H., & Tumyr, O. (2001). Microbial fractionation of carbon isotopes in altered basaltic glass from the Atlantic Ocean, Lau Basin and Costa Rica Rift. *Chemical Geology*, 173, 313–330. [https://doi.org/10.1016/S0009-2541\(00\)00285-0](https://doi.org/10.1016/S0009-2541(00)00285-0)
- Gilbert, L. A., & Bona, M. L. (2016). Permeability of oceanic crustal rock samples from IODP Hole 1256D. *Geochemistry, Geophysics, Geosystems*, 17, 3825–3832. <https://doi.org/10.1002/2016GC006467>
- Glover, P. W., Hole, M. J., & Pous, J. (2000). A modified Archie's law for two conducting phases. *Earth and Planetary Science Letters*, 180, 369–383. [https://doi.org/10.1016/s0012-821x\(00\)00168-0](https://doi.org/10.1016/s0012-821x(00)00168-0)
- Gueguen, Y., & Palciauskas, V. (1994). *Introduction to the Physics of Rocks* 294 pp. Princeton, N.J. USA: Princeton Univ. press.
- Hatakeyama, K., Lin, W., Goto, T., Hirose, T., Tanikawa, W., Hamada, Y., & Tadai, O. (2015). Experimental examination for electrical resistivity measurement using the alternative current impedance method. *Japan Agency for Marine-Earth Science and Technology Report of Research and Development*, 20, 41–50. <https://doi.org/10.5918/jamstecr.20.41> Japanese with English abstract
- Hatakeyama, K., Katayama, I., Hirouchi, K., & Michibayashi, K. (2017). Mantle hydration along outer-rise faults inferred from serpentinite permeability. *Scientific Reports*, 7, 13870. <https://doi.org/10.1038/s41598-017-14309-9>
- Jamtveit, B., Malthe-Sørensen, A., & Kostenko, O. (2008). Reaction enhanced permeability during retrogressive metamorphism. *Earth and Planetary Science Letters*, 267, 620–627. <https://doi.org/10.1016/j.epsl.2007.12.016>
- Katayama, I., Terada, T., Okazaki, K., & Tanikawa, W. (2012). Episodic tremor and slow slip potentially linked to permeability contrasts at the Moho. *Nature Geoscience*, 5, 731–734. <https://doi.org/10.1038/ngeo1559>
- Kelemen, P. B., Bach, W., Evans, K., Eslami, A., Farough, A., Hamada, M., et al. (2018). Correlated variation in vein type, vein frequency, pH, oxygen fugacity and depth in Oman Drilling Project Holes BA1B, BA3A and BA4A. In *Paper presented at American Geophysical Union Fall Meeting*, V12B-0. Washington D.C. USA.
- Kelemen, P. B., & Hirth, G. (2012). Reaction-driven cracking during retrograde metamorphism: Olivine hydration and carbonation. *Earth and Planetary Science Letters*, 345, 81–89. <https://doi.org/10.1016/j.epsl.2012.06.018>
- MacDonald, A. H., & Fyfe, W. S. (1985). Rate of serpentinization in seafloor environments. *Tectonophysics*, 116, 123–135. [https://doi.org/10.1016/0040-1951\(85\)90225-2](https://doi.org/10.1016/0040-1951(85)90225-2)
- Malvoisin, B., Brantut, N., & Kaczmarek, M.-A. (2017). Control of serpentinisation rate by reaction-induced cracking. *Earth and Planetary Science Letters*, 476, 143–152. <https://doi.org/10.1016/j.epsl.2017.07.042>
- Mavko, G., Mukerji, T., & Dvorkin, J. (2009). *The Rock Physics Handbook: Tools for Seismic Analysis of Porous Media* 524 pp. Cambridge, U.K.: Cambridge Univ. Press. <https://doi.org/10.1017/CBO9780511626753>
- Nicolas, A., Boudier, F., Ildefonse, B., & Ball, E. (2000). Accretion of Oman and United Arab Emirates ophiolite—Discussion of a new structural map. *Marine Geophysical Researches*, 21, 147–180. <https://doi.org/10.1023/A:102671802695>
- O'Hanley, D. S. (1992). Solution to the volume problem in serpentinization. *Geology*, 20, 705–708. <https://doi.org/10.1130/0091-7613>
- Paukert, A. N., Matter, J. M., Kelemen, P. B., Shock, E. L., & Havig, J. R. (2012). Reaction path modeling of enhanced in situ CO₂ mineralization for carbon sequestration in the peridotite of the Samail Ophiolite, Sultanate of Oman. *Chemical Geology*, 330–331, 86–100. <https://doi.org/10.1016/j.chemgeo.2012.08.013>
- Rudge, J. F., Kelemen, P. B., & Spiegelman, M. (2010). A simple model of reaction induced cracking applied to serpentinization and carbonation of peridotite. *Earth and Planetary Science Letters*, 291, 215–227. <https://doi.org/10.1016/j.epsl.2010.01.016>
- Shimizu, H., & Okamoto, A. (2016). The roles of fluid transport and surface reaction in reaction-induced fracturing, with implications for the development of mesh textures in serpentinites. *Contributions to Mineralogy and Petrology*, 171. <https://doi.org/10.1007/s00410-016-1288-y>
- Simpson, G., Gueguen, Y., & Schneider, F. (2001). Permeability enhancement due to microcrack dilatancy in the damage regime. *Journal of Geophysical Research*, 106, 3999–4016. <https://doi.org/10.1029/2000JB900194>
- Slagle, A. L., & Goldberg, D. S. (2011). Evaluation of ocean crustal Sites 1256 and 504 for long-term CO₂ sequestration. *Geophysical Research Letters*, 38, L16307. <https://doi.org/10.1029/2011GL048613>
- Stein, C. A., & Stein, S. (1994). Constraints on hydrothermal heat flux through the oceanic lithosphere from global heat flow. *Journal of Geophysical Research*, 99(B2), 3081–3095. <https://doi.org/10.1029/93JB02222>
- Stesky, R. M., & Brace, W. F. (1973). Electrical conductivity of serpentinitized rocks to 6 kilobars. *Journal of Geophysical Research*, 78, 7614–7621. <https://doi.org/10.1029/JB078i032p07614>
- Teagle, D. A. H., Kelemen, P. B., Matter, J. M., Templeton, A. S., & Coggon, J. A. (2018). Introduction to the Oman Drilling Project. In *Paper presented at American Geophysical Union Fall Meeting*, V13E-0151. Washington D.C. USA.
- Ulven, O. I., Jamtveit, B., & Malthe-Sørensen, A. (2014). Reaction-driven fracturing of porous rock. *Journal of Geophysical Research*, 119, 7473–7486. <https://doi.org/10.1002/2014JB011102>
- Umino, S., Ildefonse, B., Kelemen, P. B., Kodaira, S., Michibayashi, K., Morishita, T., Teagle, D. A. H., & the MoHole proponents (2012). MoHole to Mantle (M2M). In *IODP Proposal 805-MDP, International Ocean Discovery Program*. La Jolla, CA, USA. <http://www.iodp.org/proposals/active-proposals>
- Uno, M., Kasahara, H., Okamoto, A., & Tsuchiya, N. (2019). Experimental investigation of reaction-induced stress and permeability evolution in MgO-H₂O system. In *Paper presented at Japan Geoscience Union Meeting*, SCG61-14. Makuhari, Japan.
- Violay, M., Pezard, P. A., Ildefonse, B., Belghoul, A., & Laverne, C. (2010). Petrophysical properties of the root zone of sheeted dikes in the ocean crust: A case study from Hole ODP/IODP 1256D, Eastern Equatorial Pacific. *Tectonophysics*, 493(1–2), 139–152. <https://doi.org/10.1016/j.tecto.2010.07.013>
- Zheng, X., Cordonnier, B., Zhu, W., Renard, F., & Jamtveit, B. (2018). Effects of confinement on reaction-induced fracturing during hydration of periclase. *Geochemistry, Geophysics, Geosystems*, 19, 2661–2672. <https://doi.org/10.1029/2017GC007322>
- Zhu, W., Fusseis, F., Lisabeth, H., Xing, T., Xiao, X., De Andrade, V., & Karato, S. (2016). Experimental evidence of reaction-induced fracturing during olivine carbonation. *Geophysical Research Letters*, 18, 9535–9543. <https://doi.org/10.1002/2016GL070834>